Hard-X-Ray Phase-Difference Microscopy Using a Fresnel Zone Plate and a Transmission Grating

W. Yashiro,[1] Y. Takeda,[1] A. Takeuchi,[2] Y. Suzuki,[2] and A. Momose[1]

[1]*Department of Advanced Materials Science, Graduate School of Frontier Sciences, The University of Tokyo, 5-1-5 Kashiwanoha, Kashiwa, Chiba 277-8561, Japan*

[2]*Japan Synchrotron Radiation Research Institute (JASRI), 1-1-1 Kouto, Sayo-cho, Sayo-gun, Hyogo 679-5198, Japan*

(Received 20 May 2009; published 28 October 2009)

Novel hard x-ray phase imaging microscopy that simply uses an objective and a transmission grating is described. The microscope generated an image that exhibited twin features of a sample with an opposite phase contrast having a separation of a specific distance. Furthermore, the twin features were processed to generate an image mapping the x-ray phase shift through a simple algorithm. The presence of the grating did not degrade the spatial resolution of the microscope. The sensitivity of our microscope to light elements was about 2 orders of magnitude higher than that of the absorption contrast microscope that was attained by simply removing the grating. Our method is attractive for easily appending a quantitative phase-sensitive mode to normal x-ray microscopies, and it has potentially broad applications in biology and material sciences.

DOI: 10.1103/PhysRevLett.103.180801 PACS numbers: 07.85.Tt, 42.30.Va, 87.59.−e

Nondestructive and quantitative visualization of internal structures of materials with a nanometer-scale spatial resolution will bring dramatic progress in biology and material sciences. The development of hard x-ray focusing optics has made x-ray microscopy a potential candidate for such a technique [1–3]. Not only the spatial resolution of an imaging technique but also its sensitivity is a key factor that determines its performance. In conventional hard x-ray imaging, the difference in absorption among materials has been used for contrast formation, but the sensitivity is low especially when materials consisting of light elements are observed. In the early 1990s, several x-ray imaging techniques measuring the phase shift of hard x rays were proposed [4,5]; the so-called x-ray phase imaging technique has been highlighted because of its sensitivity to light elements three orders of magnitude higher than that of absorption-contrast imaging. Zernike's phase-contrast microscopy [6] has been applied for hard x rays [7,8], but the technique is not quantitative for strong-phase objects. Various other x-ray phase imaging microscopies have also been proposed [9–16], but they require specially designed x-ray optics [11,12,15] and/or a wave field that is mostly coherent on their objective [9,10,12–16].

X-ray phase imaging and tomography techniques using two transmission gratings [17–22], represented by x-ray Talbot interferometry, have attracted increasing attention. X-ray Talbot interferometry has been combined with the optics of a normal x-ray microscope to append a mode for phase sensitivity [23]. Differential phase images were quantitatively generated for weakly absorbing objects. Furthermore a three-dimensional observation through the technique of x-ray phase tomography was conducted. Although it consists of simple optics and does not require high spatial coherence, x-ray differential phase imaging using x-ray Talbot interferometry cannot realistically achieve 1000-fold sensitivity [24]. In addition, magnification reduces the sensitivity of differential phase imaging because the slope of the wave front becomes gentle. Another problem occurs wherein the spatial resolution is limited by the pitch of the gratings.

In this Letter, we describe a novel x-ray phase imaging microscope consisting of an objective and a single transmission grating. The microscope can provide a phase image without high spatial coherence and is quantitative even to strong-phase objects, which is difficult to be covered by Zerinike's phase-contrast imaging technique that is widely used with x-ray microscopy.

The method presented here also uses the self-imaging phenomenon [25] as in x-ray Talbot interferometry, but the self-image is largely magnified by placing a grating just behind the back-focal plane and resolved using an image detector. This allows us to obtain a phase *difference* image; it is not a *differential* phase image but *twin* phase images separated by a specific distance. Therefore, the method is inherently a phase imaging microscopy, which resolves the problem with the sensitivity of the x-ray Talbot interferometry, while the spatial resolution is, in principle, almost the same as that of the absorption-contrast microscopy.

Consider the setup shown in Fig. 1, where an objective, e.g., Fresnel zone plate (FZP), is illuminated by a quasi-monochromatic and quasiplane wave. A sample and a detector are put on the object and image planes. The magnification M is given by b/a (a and b are the distances from the FZP to the object and image planes). Assume that a transmission grating G_1 with a pitch of d_1 is placed at a distance R_1 downstream from the back-focal plane of the objective. We can show analytically that the focal point can be regarded as an x-ray source of a spherical wave that

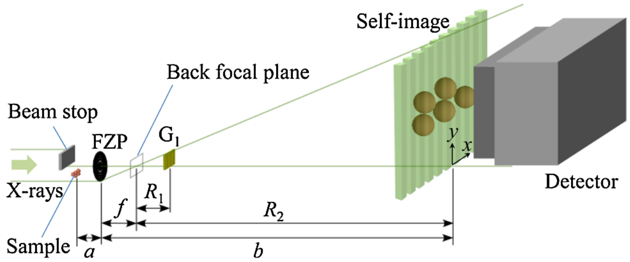

FIG. 1 (color online). Setup of phase-difference x-ray microscopy with single grating (Gl).

generates a self-image of the grating. Under spherical-wave illumination, the self-image with the Talbot order p is formed at a distance downstream from the focal point, R_2, given by

$$R_2 = \frac{{R_1}^2}{R_1 - pd_1^2/\lambda}, \tag{1}$$

where λ is an x-ray wavelength [25]. For a given R_2 (for a given M), two R_1's are allowed:

$$R_1 = \frac{R_2}{2}\left(1 \pm \sqrt{1 - 4pd_1^2/\lambda R_2}\right). \tag{2}$$

The pitch d_2 of the self-image is given by $d_1 R_2/R_1$. The case of $+$ in Eq. (2) corresponds to Ref. [23], where an amplitude grating was used at the position of the self-image because d_2 was too small to resolve directly. The present approach corresponds to the case of $-$, where d_2 was large enough to resolve. This allows us not only to skip the use of the amplitude grating but to avoid the degradation in the spatial resolution due to the diffraction by G_1 as in Ref. [23].

The wave field $E(x, y)$ on the image plane can be written in the paraxial approximation by

$$E(x, y) \approx -\frac{1}{M}\exp\left[-\frac{2\pi i}{\lambda}r\right]\sum_n a'_n \exp\left[\frac{2\pi i n x}{d_2}\right] \times E_0\left(-\frac{1}{M}(x + npd_2), -\frac{1}{M}y\right), \tag{3}$$

where r is the distance from the focal point and E_0 is the electric field just behind the sample. The factor a'_n is the nth Fourier coefficient of the amplitude of the self-image, given by $a'_n = a_n \exp[\pi i p n^2]$, where a_n is the nth Fourier coefficient of the amplitude transmission function of the grating. If the source is spatially incoherent, and the object plane is sufficiently far from the source, the intensity $I(x, y)$ on the image plane can be given by

$$I(x, y) \propto \sum_{n,m} \mu_m a'_n a'^{*}_{n+m} \exp\left[\frac{-2\pi i m x}{d_2}\right] E_{0,n} E^{*}_{0,n+m}, \tag{4}$$

where $E_{0,n}$ is defined by $E_0(-\frac{1}{M}(x + npd_2), -\frac{1}{M}y)$ and μ_m is the complex coherence factor of the x rays [26] at two points separated by a distance mpd_2/M incident on the object plane, which is derived by the Van Cittert-Zerinike theorem [27]. Note that a spatial coherence length in the x direction that is comparable to pd_2/M on the object plane is sufficient for the Talbot effect to occur if the spatial resolution that is determined by the FZP is sufficiently high compared with d_2/M.

Next, we measure $I_k(x, y)$ by displacing the grating with a step of kd_1/N in the x direction $[k = 0, 1, \ldots, N - 1 (N \geq 3)]$. Then, using the fringe-scanning method, the first order Fourier term of $I(x, y)$ is obtained [28]:

$$\sum_{k=0}^{N-1} I_k \exp\left(\frac{2\pi i k}{N}\right) \approx N\mu_1 \exp\left[\frac{-2\pi i x}{d_2}\right] \times \sum_n a'_n a'^{*}_{n+1} E_{0,n} E^{*}_{0,n+1}. \tag{5}$$

That is, interferences between neighboring orders are extracted. In practice using a grating with a Ronchi ruling is convenient. Then, even order Fourier coefficient of the amplitude transmission function except for the 0th order vanishes. As a result, only two terms of $a'_{-1}a'^{*}_0$ and $a'_0 a'^{*}_1$ in the summation of Eq. (5) remain. Consequently, image $P(x, y)$ can be obtained as follows:

$$P(x, y) = a'_{-1}a'^{*}_0 E_{0,-1}E^{*}_{0,0} + a'_0 a'^{*}_1 E_{0,0}E^{*}_{0,1}. \tag{6}$$

Note that $(a'_{-1}a'^{*}_0)^* = a'_0 a'^{*}_1$. Assuming that the sample consists of weakly absorbing material for simplicity, we can finally get a phase-difference image by taking the argument of $P(x, y)$:

$$\arg[P(x, y)] = \frac{\Phi(x_s + pd_2/M, y_s) - \Phi(x_s - pd_2/M, y_s)}{2}, \tag{7}$$

where $\Phi(x_s, y_s)$ is the phase shift by the sample and (x_s, y_s) is the coordinate on the object plane defined by $(-x/M, -y/M)$. The shearing distance of the twin features is given by pd_2 on the image plane.

If the phase-difference image is included in the field of view, a phase image $\Phi(x_s, y_s)$ is calculated using the following equation:

$$\Phi(x_s, y_s) = 2\frac{-J_1\sum_{j=-J_2}^{-1}\mathcal{P}_j + J_2\sum_{j=0}^{J_1-1}\mathcal{P}_j}{J_1 + J_2}, \tag{8}$$

where $J_1, J_2 \geq 1$, $\mathcal{P}_j \equiv \arg[P(x - (2j + 1)pd_2, y)]$, and $\Phi(x_s - 2J_1 pd_2/M) = \Phi(x_s + 2J_2 pd_2/M) = 0$ (no sample near the edges of the image) is assumed.

These theoretical results were demonstrated in an experiment performed at BL20XU in SPring-8, Japan. The x-ray beam from an undulator was monochromatized using a Si 111 double crystal monochrometer. The experimental station was located 245 m downstream from the source, the width of which was 0.4 mm in the horizontal direction (the x direction in Fig. 1). A beam stop, sample, objective, phase grating, and detector were arranged in the station, as shown in Fig. 1. A commercially available 0.7-μm-thick tantalum FZP (NTT-AT, outermost zone width: 86.6 nm, diameter: 416 μm) fabricated on a 2 μm-thick SiC membrane was used as an objective. The x-ray energy was fixed at 9 keV, and the focal length (f) of the FZP was 261 mm. To maximize the magnification, we placed the detector at a position as far as possible within the experimental space (6461 mm downstream from the FZP), and the sample was placed on the object plane (272 mm upstream from the FZP), resulting in a magnification of 23.7. An x-ray camera consisting of a phosphor screen (10 μm-P43, Gd_2O_2S:Tb+ fine powders), a relay lens, and a cooled charge-coupled device (CCD) camera (Hamamatsu Photonics C4742-98-24A, 1344×1024 pixels) was used as the detector. The effective pixel size of the detector was 4.34 μm, which corresponds to 183 nm on the object plane.

A 4.3 μm-pitch gold Ronchi grating was used. Its thickness was designed to be 0.92 μm as it works as a $\pi/2$ phase grating at 9 keV. The Talbot order was fixed at 1/2 ($R_1 = 67.8$ mm) because the effective photon number used for obtaining a phase-difference image takes a maximum at $p = 1/2, 3/2, \ldots$, and the smallest p makes the shear distance largest [21,25].

Figure 2 shows a phase-difference image of polystyrene (PS) spheres. We used a 43-step fringe scan with an exposure time of 2 sec each. The large number of steps was to avoid the systematic error due to the higher order harmonics [29]. The shear distance of the twin features was 395 μm on the detector, which agreed well with $2pd_2$ predicted through the theory described above [see Eq. (7)]. Figure 2(b) is an enlarged image of the squared area in Fig. 2(a). The filled circles in Fig. 2(c) are a section profile along the dashed line in Fig. 2(b). The solid line in Fig. 2(c) is the phase shift calculated for a PS sphere with a diameter of 5.8 μm. Here the real part of the refractive index of PS ($1 - 2.845 \times 10^{-6}$ at 9 keV) from a database [30] was used. The good agreement of the experimental data with the calculated data shows that the phase shift by the sample is quantitatively retrieved. The standard deviation of the noise in a flat field is $2\pi \times 0.003$ rad.

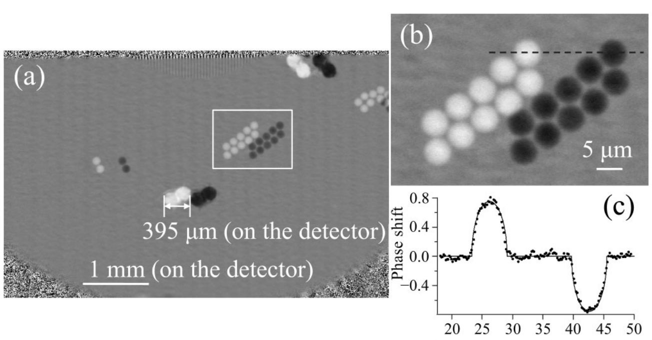

FIG. 2. Phase image of PS spheres obtained by phase-difference microscopy (gray scale: $-0.5\pi \sim 0.5\pi$). (a) Entire field of view, where scale bar is given on detector. (b) Enlarged image in square area shown in (a) (gray scale: $-0.3\pi \sim 0.3\pi$). The scale bar is given on the object plane. (c) Section profile along the line shown in (b). The filled circles are the experimental data, and the solid line is the calculated data.

When the size of the sample is less than the shear distance, as in Fig. 2, the features of the sample are phase images in themselves. Otherwise, twin phase images with different signs overlap each other, and another process [Eq. (8)] is needed. Figure 3(a) is an example, where twin phase images of a 1-μm-thick tantalum Siemens star pattern overlaps. A phase image of the Siemens star pattern was successfully retrieved from the twin images using the Eq. (8) as shown in Fig. 3(b).

The spatial resolution in the horizontal direction was estimated to be 450 nm from the edge of the Siemens star pattern shown in Fig. 3(a). The resolution was almost the same as that of the absorption-contrast image obtained simply by removing the grating. The degradation in the spatial resolution due to the grating, which was inevitable in the case of the x-ray Talbot interferometer with an FZP [23], was thus avoided.

Because no contrast was seen for the PS spheres in an absorption-contrast image (not shown), the ratio of the sensitivity of our method to that of the absorption-contrast method could not be calculated directly. Instead, we discuss the sensitivity of the method, including the theoretical aspect. Assuming that the phase shift of a sample is sufficiently small, we compare the detection limit of the phase shift in a phase-difference image [$\Delta(\Phi/2)$] with that in an absorption-contrast image [$\Delta(\mu t)$] obtained by removing the grating. If these limits are determined only by photon statistics, they are related as follows [24,31]:

$$\Delta(\Phi/2) \approx \frac{\sqrt{b_0}}{\mu_1 b_1} \Delta(\mu t), \tag{9}$$

where b_0 and $\mu_1 b_1$ are the 0th and the 1st Fourier coefficients of the intensity of the self-image normalized by the intensity when the grating is removed. In the case of Fig. 2, b_0 and $\mu_1 b_1$ were experimentally estimated to be 0.49 and

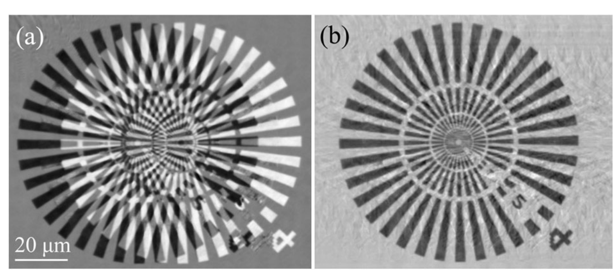

FIG. 3. Phase images of 1-μm-thick Ta Siemens star pattern. (a) Phase-difference image with overlapped features of opposite contrast and (b) retrieved phase image constructed from (a).

0.27. The standard deviations of the noise in Fig. 2 and that in an absorption-contrast image obtained without the grating were 0.019 and 0.0075, respectively, which are consistent with Eq. (9). Once Eq. (9) is confirmed to be correct, we can obtain the relationship between the detection limits of the real part $(1-\delta)$ and the imaginary part (β) of the refractive index ($\Delta\delta$ and $\Delta\beta$):

$$\Delta\delta \approx \frac{2\sqrt{2b_0}}{\mu_1 b_1}\Delta\beta. \tag{10}$$

In terms of the signal-to-noise ratio,

$$\frac{\delta}{\Delta\delta}:\frac{\beta}{\Delta\beta} \approx 1:\frac{2\sqrt{2b_0}}{\mu_1 b_1}\frac{\beta}{\delta} \tag{11}$$

is found. Because δ is 3 orders of magnitude larger than β for light elements, we concluded that the method presented here has a sensitivity about 2 orders of magnitude higher than that of the absorption-contrast imaging.

In summary, novel x-ray phase imaging microscopy, which simply consists of an objective and a transmission grating, was formulated based on the Talbot effect. Phase-difference images (twin phase images) could be generated in an experiment using synchrotron radiation. The sensitivity in the phase-difference image was about 2 orders of magnitude higher than that of the absorption-contrast x-ray microscopy that was attained by removing the grating, while the spatial resolution was almost the same as that of the absorption-contrast microscopy. Retrieval of a phase image from twin phase images was also demonstrated. Our approach is attractive for easily appending a phase-sensitive mode to normal x-ray microscopes, and its quantitativity should make it possible for x-ray phase tomography to be performed in near future. Thus our approach will provide a powerful way in biology and material science to visualize internal structures with a nanometer-scale spatial resolution.

The experiment was performed at SPring-8 (proposal number 2008B1596). This study was financially supported by Grants-in-Aid for Scientific Research (B) (19360027) from the Ministry of Education, Culture, Sports, Science and Technology.

[1] M. Zwanenburg *et al.*, Physica (Amsterdam) **283B**, 285 (2000).
[2] C. Schroer *et al.*, Appl. Phys. Lett. **87**, 124103 (2005).
[3] H. C. Kang *et al.*, Appl. Phys. Lett. **92**, 221114 (2008).
[4] R. Fitzgerald, Phys. Today **53**, No. 7, 23 (2000).
[5] A. Momose, Jpn. J. Appl. Phys. **44**, 6355 (2005).
[6] G. Schmahl *et al.*, Rev. Sci. Instrum. **66**, 1282 (1995).
[7] Y. Kagoshima *et al.*, Jpn. J. Appl. Phys. **40**, L1190 (2001).
[8] J. R. Izzo, Jr. *et al.*, J. Electrochem. Soc. **155**, B504 (2008).
[9] W. Leitenberger *et al.*, Opt. Commun. **180**, 233 (2000).
[10] W. Leitenberger and A. Snigirev, J. Appl. Phys. **90**, 538 (2001).
[11] T. Wilhein *et al.*, Appl. Phys. Lett. **78**, 2082 (2001).
[12] T. Koyama *et al.*, Jpn. J. Appl. Phys. **43**, L421 (2004).
[13] Y. Suzuki and A. Takeuchi, Rev. Sci. Instrum. **76**, 093702 (2005).
[14] N. Watanabe *et al.*, in *IPAP Conference Series* (IPAP, Tokyo, 2006), Vol. 7, p. 372.
[15] T. Koyama *et al.*, Jpn. J. Appl. Phys. **45**, L1159 (2006).
[16] Y. Suzuki and A. Takeuchi, Jpn. J. Appl. Phys. **47**, 8595 (2008).
[17] A. Momose *et al.*, Jpn. J. Appl. Phys. **42**, L866 (2003).
[18] F. Pfeiffer *et al.*, Nature Phys. **2**, 258 (2006).
[19] F. Pfeiffer *et al.*, Nature Mater. **7**, 134 (2008).
[20] Y. I. Nesterets and S. W. Wilkins, Opt. Express **16**, 5849 (2008).
[21] A. Momose, W. Yashiro, and Y. Takeda, in Biomedical Mathematics: Promising Directions in Imaging, Therapy Planning and Inverse Problems, edited by Y. Censor, M. Jiang, and G. Wang (Medical Physics Publishing, Madison, WI, to be published).
[22] Z.-F. Huang *et al.*, Phys. Rev. A **79**, 013815 (2009).
[23] Y. Takeda *et al.*, Appl. Phys. Express **1**, 117002 (2008).
[24] A. Momose, W. Yashiro, and Y. Takeda, Jpn. J. Appl. Phys. **47**, 8077 (2008).
[25] K. Patorski, in *Progress in Optics XXVII*, edited by E. Wolf (Elsevier Science Publishers B.V., Amsterdam, 1989).
[26] J. W. Goodman, *Statistical Optics* (Wiley-Interscience, New York, 2000).
[27] Exactly speaking, we defined μ_m by the complex coherence factor without the space-variant phase factor. Even in the case where the space-variant phase factor has to be taken into account, it can be included in E_0's in Eq. (4).
[28] J. Bruning *et al.*, Appl. Opt. **13**, 2693 (1974).
[29] K. Stetson and W. Brohinsky, Appl. Opt. **24**, 3631 (1985).
[30] http://henke.lbl.gov/optical_constants/.
[31] W. Yashiro, Y. Takeda, and A. Momose, J. Opt. Soc. Am. A **25**, 2025 (2008).